Research Square

Preprints are preliminary reports that have not undergone peer review.
They should not be considered conclusive, used to inform clinical practice,
or referenced by the media as validated information.

The Use of Hyaluronic Acid in a 3D Biomimetic Scaffold Supports Spheroid Formation and the Culture of Cancer Stem Cells.

Gamze Demirel

gamze.demirel@ogr.iu.edu.tr

Istanbul University Institute of Science

Yaprak Donmez Cakıl

Maltepe University

Gursel Koltuk

Yildiz Technical University Institute of Science

Ranan Gulhan Aktas

Maltepe University

Mahmut Calıskan

Istanbul University Institute of Science

Article

Keywords: Hyaluronic acid, Stem cells, Spheroids, Three-Dimensional Cell Culture, Biometerials

Posted Date: April 17th, 2024

DOI: https://doi.org/10.21203/rs.3.rs-4226662/v1

License: This work is licensed under a Creative Commons Attribution 4.0 International License.
Read Full License

Additional Declarations: No competing interests reported.

Abstract

Three-dimensional (3D) bioprinting culture models capable of reproducing the pathological architecture of diseases are increasingly advancing. In this study, 3D scaffolds were created using extrusion-based bioprinting method with alginate, gelatin, and hyaluronic acid to investigate the effects of hyaluronic acid on the physical properties of the bioscaffold as well as on the formation of liver cancer spheroids. Conformational analysis, rheological characterization, and swelling-degradation tests were performed to characterize the scaffolds. After generating spheroids from hepatocellular carcinoma cells on the 3D scaffolds, cell viability and proliferation assays were performed. Flow cytometry and immunofluorescence microscopy were used into examine the expression of albumin, CD44, and E-cadherin to demonstrate functional capability and maturation levels of the spheroid-forming cells. The results show that hyaluronic acid in the scaffolds correlates with spheroid formation and provides high survival rates. It is also associated with an increase in CD44 expression and a decrease in E-cadherin, while there is no significant change in the albumin expression in the cells. Overall, the findings demonstrate that hyaluronic acid in a 3D hydrogel scaffold supports spheroid formation and may induce stemness. We present a promising 3D scaffold model for enhancing liver cancer spheroid formation and mimicking solid tumors. This model also has the potential for further studies to examine stem cell properties in 3D models.

Introduction

Three-dimensional (3D) cell culture enables cells to grow in an environment that more closely resembles to their natural tissue environments. Thus, it allows cells to grow and develop more realistically, enabling the accurate monitoring of cell metabolism, function, and behavior [1]. 3D cell culture is also used to investigate intercellular interactions, cell migration, cell-matrix interactions, and even virus infections [2]. The primary goal of three-dimensional cell culture is the formation of cell aggregates, known as spheroids. Spheroids are clusters of cells formed by self-assembly in an environment that prevents attachment to a flat surface [3]. For spheroid formation, communication between membrane proteins (integrins) and extracellular matrix (ECM) proteins is necessary [4]. Initially, dispersed cells aggregate due to long-chain ECM fibers containing Arginylglycylaspartic acid (RGD) motifs, which allow binding to cell surface integrins, serving as a recognition system for cell adhesion, leading to increased cadherin expression [5]. As cadherin accumulates on the cell membrane surface, homophilic is a cell adhesion molecule crucial for the formation of zonula adherens [6]. Cadherin accumulates on the cell membrane surface, and homophilic cadherin-cadherin binding between adjacent cells allows for tightening of connections between cells, resulting in spheroid formation [7].The ability to control cell movement in three-dimensional cell culture is crucial for understanding developmental mechanisms, tracking tumor formation stages, and conducting research in the fields of regenerative medicine and cancer biology [8,9].

3D bioprinting endeavors represent promising 3D cell culture systems for generating complex biological structures in tissue engineering and regenerative medicine. The goal is to alleviate the limitations of

traditional tissue engineering methods by precisely and controllably layering biomaterials into the desired 3D model. In this study, 3D scaffolds were created using extrusion-based bioprinting method with alginate, gelatin, and hyaluronic acid. Sodium alginate is a natural polysaccharide found naturally in seaweeds, marine shellfish, and other marine organisms [10]. Due to its properties such as biocompatibility, biodegradability, non-immunogenicity, and chelating ability, alginate is widely used in tissue engineering, drug delivery, and various biomedical applications. Gelatin, a single-chain polymer, is a natural biomaterial obtained from the partial hydrolysis and breakdown of collagen's triple helical structure extracted from the bones, cartilage, and skin of some animals [11,12]. Widely used as a biomaterial, gelatin is biocompatible with all cell types. Since gelatin possesses a structure that can be biologically degraded, it is suitable for tissue remodeling and regeneration [13]. Gelatin contains the tripeptide motif Arg-Gly-Asp, which is recognized by integrins on the cell membrane, allowing cells to bind to it. Hyaluronic acid (HA) is a natural polysaccharide and an unsulfated glycosaminoglycan proteoglycan complex that is a part of the ECM [14]. Increased HA content in the cancer microenvironment supports tumor progression [15]. The role of HA in cancer progression arises from its interaction with cell surface receptors, which support intracellular signal transduction associated with cellular differentiation, survival, proliferation, migration, angiogenesis, and resistance to therapeutic molecules [14,16]. Cell surface receptors for HA-mediated mobility are known as CD44. HA on the cell surface can facilitate the attachment of spreading carcinoma cells to distant lymph nodes or endothelial cells, thereby increasing the likelihood of metastasis [17]. Additionally, HA plays an active role in tumor growth and tumor metastasis [15]. The necessity to pre-coat surfaces with proteins demonstrates the requirement for HA to facilitate cell adhesion with biomaterials. Tumor spheroids produced in HA-based structures can replicate the 3D architecture of tumors and also mimic the cell-HA signaling present in the tumor microenvironment [18].

In this study, we developed a 3D scaffold model printed using 3D AlgGel hydrogels to create an extracellular microenvironment that enhances cancer cell viability and stemness. We performed mechanical and conformational characterization of the hydrogels. Cancer spheroids were generated, and we determined the cell viability as well as the expression of CD44, E-cadherin, and albumin using flow cytometry and immunofluorescence.

Materials and Methods

Materials

Hyaluronic Acid (1.8 MDa), Anti-Human Albumin antibody, calcium chloride ($CaCl_2$), Dulbecco's Modified Eagle Medium (DMEM), were purchased from Sigma-Aldrich (USA). Sodium alginate (MW 50000 Da) from Isolab (Germany), and gelatin (MW ~ 50,000–100,000 Da) from Neofroxx (Germany) were obtained to create scaffolds. CD44 Monoclonal Antibody, LIVE/DEAD™ Cell Imaging Kit (488/570), Trypsin-EDTA (0.25%), Penicillin-Streptomycin (10,000 U/mL), and Goat anti-Rabbit IgG (H + L) Secondary Antibody, DyLight™ 488 were purchased from Thermo Scientific (USA). Cello-IF solution for immunofluorescence staining was obtained from Cellorama (USA).

Preparation of hydrogels

The sodium alginate and gelatin powders, in powdered form, were sterilized by exposure to UV light for 1 hour. The powders were then dissolved in distilled water (dH_2O) and mixed using a magnetic hotplate stirrer at 37°C for 1 hour and at room temperature for 30 minutes to obtain a homogeneous composite precursor as indicated in Table 1. Based on reference studies conducted within the created hybrid hydrogel, the composition of the hybrid hydrogel was determined to be 3% alginate and 8% gelatin. The resulting hydrogel was transferred into centrifuge tubes and centrifuged at 1500 rpm for 15 minutes to eliminate air bubbles. It was then stored in a refrigerator at 4°C and used within one week. A 100 mM calcium chloride ($CaCl_2$) solution was prepared by dissolving $CaCl_2$ in water and stored at 4°C in the refrigerator until use to cross-link the alginate. Preparation of all materials for biological testing was always carried out under sterile conditions.

Table 1
Composition of prepared hydrogel samples.

Hydrogel name	% HA (*w/v*)	% Gelatin (*w/v*)	% Alginate (*w/v*)
2%HA-Gel-Alg	2	8	2
1%HA-Gel-Alg	1	8	3
0,5%HA-Gel-Alg	0,5	8	3
0%HA-Gel-Alg	0	8	3

Printing of the scaffold

Printing of the hydrogel was performed using a 3D bioprinter (Axolotl, Turkey). The hydrogels were loaded into 3 ml printing cartridges and connected to a controllable pressure regulator (0–72 psi). The printing flow rate of the hydrogel was optimized by adjusting the extrusion pressure (5–13 psi) and the Z-axis from the nozzle tip to the printing bed was set to 0.1 mm. Prior to printing, the hydrogels were removed from + 4°C and allowed to equilibrate at room temperature for 3 hours. A three-layer scaffold (10 x 10 x 1 mm) was printed onto a petri dish using a 25 G nozzle (320 µm diameter). The dimensions of the 3D printed scaffolds were measured after cross-linking with $CaCl_2$. Scaffolds were printed with all hydrogel mixtures to measure the line width (n = 5).

Fourier Transform Infrared Spectroscopy (FT-IR)

A physico-chemical experiment was conducted using FT-IR spectroscopy to confirm the presence of alginate and gelatin in our hydrogels. The chemical composition was verified by Fourier Transform Infrared Spectroscopy. The chemical composition was analyzed using the Spectrum One FT-IR

Spectrometer (PerkinElmer, Shelton, USA). An FTIR-ATR spectrophotometer (Nicolet 6700/Smart iTR, Thermo Scientific) was used for analysis; the results were plotted in the wavelength range of 4000 to 550 cm^{-1}.

Rheological Characterization

Dynamic viscosity analyses were conducted using a DV3T RV rheometer (Brookfield, Massachusetts, USA) to determine the shear rate curve against viscosity for mechanical characterization of the hydrogel. Additionally, rotational viscosity analyses were performed using a Discovery HR20 Rheometer (TA Instruments, New Castle, Delaware, USA) equipped with 25 mm aluminum parallel plate geometry.

Swelling Test

The liquid absorption of the hydrogels was evaluated using gravimetric technique. Approximately 0.5 g (W_0) of hydrogel was incubated in 10 mL of DMEM/PBS for 10 days to reach equilibrium swelling. After removing excess liquid, the weight of the swollen hydrogel (W_s) was measured.The following equation was used to determine the swelling ratio (SR) of scaffold sample [19].

$SR\ (\%) = (W_s - W_0 / W_0) \times 100$

Cell Viability

Cell viability was examined using the Live-Dead Imaging Kit (Thermo Scientific). In brief, cells on the scaffold were stained with 2 µM calcein AM/4 µM BOBO Iodide at 37°C in 5% CO_2 for 15 minutes. The cell-loaded scaffolds were washed twice with serum-free medium, and images were captured using an LSM 700 confocal microscope (Zeiss, Germany). The percentage of live and dead cells was determined by counting cells using Image-J software (USA), and a histogram was created to compare cell viability among different printed groups.

Immunofluorescence Staining

A whole mount immunofluorescent staining was performed to label the spheroids ion the scaffolds. The spheroids within the scaffolds were fixed with 4% formaldehyde at 37°C for 15 minutes and then washed three times with CelloIF. The spheroids were incubated with the primary antibodies specific for E-cadherin, CD44, and albumin for 1 hour. They were washed with CelloIF three times. Subsequently, they were incubated for 1 hour with AlexaFluor488nm and AlexaFluor550nm conjugated secondary antibodies diluted in CellO-IF. After incubation, they were washed three times with phosphate-buffered saline (PBS). The labeled spheroids in scaffolds were coated with a mounted medium including glycerol, PBS, and the nuclear stain DAPI. The samples were analyzed using a LSM 700 confocal microscope.

Flow Cytometry Analysis

After 10-day incubation, spheroids were harvested from AlgGel scaffolds using trypsin enzyme and prepared for flow cytometric evaluation. Experimental groups with HA concentrations of 2%, 1%, 0.5%, and 0% were washed with phosphate-buffered saline (PBS) and then incubated at 37°C for 1 hour with

CD44 (1:200 dilution), E-cadherin (1:100 dilution), and Albumin (1:50 dilution) antibodies. After two washes with PBS, specimens were labeled with the matching secondary antibodies conjugated with Alexa Fluor 488nm and Alexa Fluor 550nm. Subsequently, they were washed twice with phosphate-buffered saline (PBS), suspended again in PBS for measurement, and analyzed with BD FACSCalibur (BD Biosciences, San Diego, CA, USA). At least 10,000 events were collected for analysis. The obtained data were analyzed using floreada.io software.

Statistical Analysis

All data are expressed as mean ± standard deviation (SD). One-way ANOVA test was used for comparisons within groups, and Two-way ANOVA test was used for comparisons between two different groups. GraphPad Prism V.8.01 (GraphPad Software, USA) was utilized for generating bar graphs and conducting statistical analyses. A significance level of α = 0.001 was employed.

Results

Morphological Characterization of the Scaffold

The scaffold printed using a three-dimensional bioprinter was initially created as a 3D honeycomb model, which can be viewed from the x, y, and z planes in .stl format. (Fig. 1-a,c,d) The pore size is generally considered optimal between 100 to 500 µm as described in previous studies. According to the results measured using the Image J image analysis software, Measurements with the Image J analysis software demonstrated that the pore sizes of the scaffolds were between 360–370 µm. (Fig. 1, b)

Conformational Analysis of the Scaffold

The FTIR spectra of AlgGel scaffolds with 2% HA, 1% HA, and 0.5% HA ratios are shown in Fig. 2. Alginate FTIR spectrum contains five characteristic bands [22]. The bands at 1025 cm^{-1} and shoulder at 1032 cm^{-1} are associated with C-C and C-O stretching vibrations and may also be attributed to the presence of cross-linking. The asymmetric and symmetric stretching vibrations of carboxylic groups (-COO–) in alginate occur at 1600 and 1425 cm^{-1}, respectively. These peaks shift due to the interaction of alginate with other hydrogel components that do not participate in the Ca_2 + cross-linking regime. The broad absorption band between 3300–3700 cm^{-1} represents O-H stretching,[22–25] while the C-H band around 2850–3000 cm^{-1} is associated with alginate [22,24]. (Fig. 2,a)

In the FTIR spectrum, the characteristic features of gelatin are observed as follows: The wavelengths corresponding to the stretching and bending modes of the amid bonds (NH), which are a distinct feature of gelatin's protein structure, are typically found in the range of 1650 – 1550 cm-[1]. The peak at 1620–1630 cm^{-1} indicates the presence of an amid I band corresponding to the stretching vibrations of C-O and CN groups of elatin NH groups. The Amid II band is observed as a small peak at 1545–1555 cm^{-1}, and the Amid III band is observed between 1300 and 1200 cm^{-1}. This band is associated with the

stretching vibration of NH in proteins. The Amid III band is typically situated between the Amid I and Amid II bands and often appears as a smaller peak. (Fig. 2, b)

The FTIR spectrum of HA typically exhibits characteristic bands at specific wavelengths. The wavelengths corresponding to the stretching modes of O-H (hydroxyl) groups are typically found in the range of approximately 3400 – 3200 cm^{-1}. Additionally, the wavelengths corresponding to the stretching modes of C-H (alkyl) groups can be found in the range of approximately 3000 – 2800 cm^{-1}. The wavelengths corresponding to the stretching modes of C = O (carbonyl) groups can be observed in the range of approximately 1750 – 1650 cm^{-1}. (Fig. 2, c) When looking at the graph in Fig. 2-d below, similar results are observed in the respective wavelength ranges, indicating the chemical presence of HA.

Rheological Characterization of the Scaffold

To assess the suitability of adding HA to the AlgGel hydrogel, samples with the highest HA ratio of 2% HA were subjected to rheological analysis without crosslinking, as shown in Fig. 3. The AlgGel hydrogel containing 2% HA exhibited a slowly relaxing system with viscoelastic properties; thus, the storage modulus was higher than the loss modulus at all tested frequency ranges, indicating the preservation of hydrogel elasticity. (Fig. 3, a)

Comparisons can be made between the time, angular displacement, and pressure values for the given points. Based on these comparisons, significant differences in the material's response to deformation can be observed. Point 6, characterized by a time of 39.6158 s, angular displacement of 7.64106e-5 rad, and a pressure of 0.108343 MPa. Point 5, on the other hand, characterized by a time of 32.9766 s, angular displacement of 4.95551e-5 rad, and a pressure of 0.100560 MPa. The longer time at point 6 compared to point 5 suggests exposure to prolonged deformation. In this context, it can be speculated that due to the elastic properties of gelatin, the material resists prolonged deformations, alginate may respond more quickly, and hyaluronic acid may maintain its elastic properties during prolonged deformations. (Fig. 3, b)

The angular displacement of both points is similar, but point 6 has slightly greater angular displacement. This indicates that the material undergoes more shape changes during this time frame. Additionally, the lower angular displacement at point 5 suggests that the material undergoes less shape change during this time frame. Considering the characteristic properties of the material composition, gelatin may support large angular displacements due to its flexible and elastic properties, alginate may respond more limitedly, and hyaluronic acid may respond flexibly to large angular displacements.

Swelling and degradation

The swelling properties of hydrogels were evaluated after 10 days in PBS solution at 37°C (Fig. 4). AlgGel hydrogel, due to its hydrophilic nature, exhibits excellent liquid absorption capacity. After being cross-linked with $CaCl_2$, AlgGel hydrogel coated with 2%, 1%, and 0.5% HA concentrations was also incubated in PBS for 10 days. (Fig. 4, a). The swelling ratio slightly decreased after cross-linking with $CaCl_2$ due to the gelation of the hydrogel, but the balanced liquid transfer was maintained thanks to the porous structure of the scaffold. According to the measured results, increasing HA concentration did not affect pore size,

resulting in similar levels of liquid uptake within the scaffold. As of the 10th day, they exhibited maximum swelling ratios of 84%, 76%, 68%, and 50%, respectively. (Fig. 4, b).

In Vitro Compatibility of the Scaffold

To enable comparative evaluation of the proliferation rate of HepG2 cells and the morphological changes observed in response to the HA content in the environment, live images were recorded under an inverted phase-contrast microscope (Primovert, Zeiss). (Fig. 5 – a,b,c,d) As seen in the scaffold with a 2% HA ratio, larger and more distinct spheroids were formed. (Fig. 5, a) The images in Fig. 5, indicate that spheroid formation is directly proportional to the increase in HA content.

Live/Dead analysis was performed to determine the biocompatibility of scaffolds with different HA ratios. In this study, live/dead analyses were conducted to evaluate the biocompatibility of scaffolds with different hyaluronic acid (HA) ratios. Live/Dead analyses conducted on scaffolds with different HA ratios revealed a significant effect of HA ratio on cell viability within the scaffolds. As seen in Fig. 6, it was observed that as the HA ratio decreased, cell viability within the scaffolds also decreased.

The Effect of HA Ratio on E-cadherin, CD44, and Albumin Expressions

HepG2 cells were cultured in AlgGel scaffolds with different HA ratios for 10 days. On the 10th day, HepG2 cells fixed with 4% PFA were subjected to measurement of CD44, E-cadherin, and albumin expressions using confocal microscopy and flow cytometry. Figure 7 – a,b,c shows the histogram images of flow cytometer results for CD44, E-cadherin, and albumin in panels a, b, and c, respectively. Figure 7d, e, and f depict the corresponding statistical results. According to the obtained data, an increase in the HA ratio is associated with an increase in CD44 levels, while conversely, an increase in the HA ratio results in a decrease in E-cadherin levels. No significant change was observed in albumin levels.

Expression of CD44, E-cadherin, and Albumin within spheroids were examined comparatively (Fig. 8a, b, and c). The results indicated an increase at the CD44 expression and a decrease in E-Cadherin while the HA concentration gets higher in the hydrogel. The results were confirmed with flow cytometry (Fig. 8d, e, and f) and found statistically meaningful.

Discussion

The bioprinter has made significant advancements among three-dimensional cell culture systems. However, the biomaterials that are ideal for both printing and the development of cellular microenvironments are limited or expensive[30]. Commercial biomaterials, however, fail to fully replicate ECM components, resulting in cells printed with these scaffolds being unable to exhibit behaviors similar to those in their natural environment [31]. In this study, an appropriate ratio of hyaluronic acid was investigated to support cellular viability and function by combining easy-to-use natural polymers,

alginate, and gelatin in bioprinting. Additionally, the effect of HA on scaffold characterization was reported.

The hydrogel content created using alginate and gelatin biomaterials had an alginate concentration ranging from 3–7%, while the gelatin concentration was between 6% and 8%. It was demonstrated that hydrogels printed at these ratios exhibited suitable biocompatibility and mechanical characterization [32–34]. In this study, similarly to reference studies, a hydrogel containing 3% alginate and 8% gelatin (AlgGel) facilitated the creation of 3D scaffolds with good workability and shape retention at room temperature.For tissue engineering studies, the porosity and pore size of scaffolds are among the most important factors to consider when determining the effectiveness of the scaffold. This is because pore size is closely associated with cellular survival processes such as oxygen and nutrient exchange and waste removal. These functions cannot occur in a scaffold without pores, and the absence of pores can significantly decrease cellular activation in the relevant damaged tissues [22]. The incorporation of HA into the three-dimensional honeycomb-shaped scaffold created with alginate and gelatin provided a smooth surface. Changes in the HA concentration did not affect the pore size or shape. The concentrations of alginate and gelatin in the scaffold were not altered because modifying the concentrations of these biomaterials would impact the pore size and the shape of the three-dimensional model. This phenomenon has also been observed in similar studies in the literature [22,35].

The addition of hyaluronic acid at ratios of 2%, 1%, 0.5%, and 0% did not affect the mechanical characterization of the AlgGel scaffold. All formulations exhibited fluidic properties rather than elastic properties before crosslinking. This indicates that the materials could flow in the viscous/liquid phase. Even after crosslinking with CaCl2, particularly the scaffold with the highest HA ratio, maintained its integrity without fracturing, demonstrating its resilience. Rheological analyses demonstrate that the material can be easily processed and has the capability to retain desired shapes. Additionally, the material exhibits excellent mechanical stability, thereby supporting cellular growth in a suitable environment by preserving its structural integrity. The favorable flow properties of the material facilitate integration during bioprinting, providing a suitable structural framework for use in bioprinting processes. In this context, how a structure containing gelatin, alginate, and hyaluronic acid can create a stable scaffold for scaffold formation is closely related to the rheological motion changes. The contribution of gelatin in the linear viscoelastic region may enhance the mechanical durability of the scaffold for scaffold formation. This indicates that the artificially prepared extracellular matrix for the study positively influences the durability and stability of the scaffold. The shear-thinning behavior of materials like alginate and hyaluronic acid supports the increase in the scaffold's deformability and ability to take on a specific shape, crucial for better integration with cells. Additionally, the region corresponding to the parabolic rise in the material's viscoelastic properties and the linear breakage indicates that the adaptive properties of the scaffold are at a sufficient level for the study. All these material combinations' graphical reflections show that the scaffold is suitable for providing a conducive environment for cellular adhesion, migration, and growth, and it possesses an advantage in terms of compatibility with biological systems.

Scaffolds aim to create supportive microenvironments by mimicking the ECM structure, thereby facilitating cell viability and function.The number of spheroids formed within the scaffolds decreased proportionally with decreasing HA ratio. To investigate the contribution of HA to spheroid formation, HepG2 cells were cultured without scaffolds and only HA was added to the culture medium, resulting in rapid spheroid formation starting from the 3rd day. Thus, an increase in HA ratio led to higher cell organization and spheroid formation within the scaffolds.

HA, known as a direct cell surface receptor and also indicating an increase in the CD44 cancer stem cell marker, suggests an increase in cell carcinogenicity. Additionally, it plays a significant role in cell adhesion, migration, and inflammation [36]. CD44 is expressed in many cancer types and serves as a cell surface receptor regulating the metastatic ability of cancer cells [37]. Hyaluronic acid (HA) is a glycosaminoglycan found in the ECM and is considered the primary ligand for CD44, capable of binding CD44 isoforms ubiquitously. Furthermore, the binding of CD44 and HA is known to play important roles in cell-cell interactions, cell adhesion, invasion/metastasis, and is expressed in tumor-initiating cells [38]. Additionally, the HA-CD44 interaction induces changes in the cell cytoskeleton that support tumor cell motility and invasion [39]. The epithelial (E) cadherin glycoprotein, which plays a role in cellular adhesion, is a cell-cell adhesion glycoprotein [40]. The downregulation of E-cadherin during spheroid development may be associated with reduced intercellular adhesion. It is well known that the cell-cell adhesion mediated by E-cadherin contributes to contact inhibition and tumor suppression. However, the reduction of cell-cell adhesion as a result of downregulation of E-cadherin is often associated with invasive and tumor development. E-cadherin has been proposed as a prognostic marker [41]. The expression of CD44 and E-cadherin, which have different roles in cell-cell adhesion and cell-extracellular matrix (ECM) adhesion, serves as prognostic markers in tumor development[42,43]. Studies have reported that as the expression of E-cadherin decreases, the expression of CD44 may increase, and this is associated with weakening of cell-cell connections and increased metastatic capabilities of the cells [44–46]. In addition to these, this study also investigated the expression level of albumin. Albumin plays a significant role in protein synthesis, one of the fundamental functions of the liver, and is considered an indicator of liver health. Therefore, determining the expression of albumin in HepG2 spheroids or cells within AlgGel scaffolds is important to understand their ability to produce albumin and to identify any changes associated with pathological conditions such as liver cancer. This could be considered as a step towards contributing to potential therapeutic strategies 30.

The contribution of HA to spheroid formation and cancer stem cell development highlights the scaffold using the highest percentage of HA, particularly at a 2% ratio.

Conclusion

In this study, the effect of hyaluronic acid on accelerating spheroid formation in human hepatocellular carcinoma was investigated. Spheroid formation was accelerated by adding hyaluronic acid to a three-dimensional scaffold printed with bioprinting technology using the two most commonly used natural

polymers, alginate and gelatin. We demonstrated that the 3D model created with the effect of hyaluronic acid provides more favorable conditions for maintaining cell proliferation by accelerating spheroid formation. Additionally, our results exhibited effects of hyaluronic acid that support the regulation and enhancement of stem cell regeneration property. The expression of the CD44 cancer stem cell marker increased with the increase in the amount of hyaluronic acid. Our research suggests that the hyaluronic acid-supported 3D AlgGel scaffold promotes spheroid formation and stem cell expression, and can be utilized as a model 3D scaffold in various tissue engineering or drug research studies.

Declarations

Acknowledgement

This study was supported by the Istanbul University Scientific Research Projects Coordination Unit (Project ID: 39773).

Author Contributions

G.D. conceived and created the experimental design. **G.D., Y.D.C.** and **G.K.** Contributed reagents/materials/analysis tools. **G.D. and Y.D.C.** carried out the experiments. **G.D., Y.D.C.** and **G.K.** analysed and interpreted the results. **G.D.** drafted the initial manuscript**. R.G.A.** and **M.C.** read, revised, and approved the final submitted manuscript.

Data and materials availability

All data associated with this study are present in the paper or in the Supplementary Materials.

Competing interests

The authors declare no competing interests.

Corresponding author

Correspondence to Mahmut Calıskan.

References

1. Datta, P., Dey, M., Ataie, Z., Unutmaz, D. & Ozbolat, I. T. 3D bioprinting for reconstituting the cancer microenvironment. *npj Precision Oncology* vol. 4 Preprint at https://doi.org/10.1038/s41698-020-0121-2 (2020).
2. Vining, K. H. & Mooney, D. J. Mechanical forces direct stem cell behaviour in development and regeneration. *Nature Reviews Molecular Cell Biology* vol. 18 728–742 Preprint at https://doi.org/10.1038/nrm.2017.108 (2017).

3. Ryu, N. E., Lee, S. H. & Park, H. Spheroid culture system methods and applications for mesenchymal stem cells. *Cells* vol. 8 Preprint at https://doi.org/10.3390/cells8121620 (2019).
4. Sant, S. & Johnston, P. A. The production of 3D tumor spheroids for cancer drug discovery. *Drug Discovery Today: Technologies* vol. 23 27–36 Preprint at https://doi.org/10.1016/j.ddtec.2017.03.002 (2017).
5. Lin, R. Z. & Chang, H. Y. Recent advances in three-dimensional multicellular spheroid culture for biomedical research. *Biotechnology Journal* vol. 3 1172–1184 Preprint at https://doi.org/10.1002/biot.200700228 (2008).
6. Alimperti, S. & Andreadis, S. T. CDH2 and CDH11 act as regulators of stem cell fate decisions. Stem Cell Res 14, 270–282 (2015).
7. Zhang, H., Cui, X. & Hartanto, Y. Advances in multicellular spheroids formation. doi:10.1098/rsif.2016.0877.
8. Bruno, R. D. & Smith, G. H. Reprogramming non-mammary and cancer cells in the developing mouse mammary gland. Semin Cell Dev Biol 23, 591–598 (2012).
9. Sachs, P. C., Mollica, P. A. & Bruno, R. D. Tissue specific microenvironments: A key tool for tissue engineering and regenerative medicine. *Journal of Biological Engineering* vol. 11 Preprint at https://doi.org/10.1186/s13036-017-0077-0 (2017).
10. Urtaza, U.; ; *et al.* A Study of the Printability of Alginate-Based Bioinks by 3D Bioprinting for Articular Cartilage Tissue Engineering. Polymers 2022, *Vol. 14, Page 354* 14, 354 (2022).
11. DEMİREL, G. Karaciğer hücreleri ve organoidlerin üç boyutlu kültürlerinde kullanılmak üzere geliştirilmiş biyomalzemeler. Frontiers in Life Sciences and Related Technologies 2, 111–119 (2021).
12. Gheorghita, R., Anchidin-Norocel, L., Filip, R., Dimian, M. & Covasa, M. Applications of Biopolymers for Drugs and Probiotics Delivery. Polymers (Basel) 13, (2021).
13. Wang, X. *et al.* Gelatin-Based Hydrogels for Organ 3D Bioprinting. Polymers (Basel) 9, (2017).
14. Toole, B. P. Hyaluronan: from extracellular glue to pericellular cue. *Nature Reviews Cancer 2004 4:7* 4, 528–539 (2004).
15. Rooney, P., Kumar, S., Ponting, J. & Wang, M. The role of hyaluronan in tumour neovascularization (review). Int J Cancer 60, 632–636 (1995).
16. Auvinen, P. *et al.* Hyaluronan in peritumoral stroma and malignant cells associates with breast cancer spreading and predicts survival. Am J Pathol 156, 529–536 (2000).
17. W Bourguignon, L. Y., Wong, G., Earle, C., Krueger, K. & Spevak, C. C. Hyaluronan-CD44 Interaction Promotes c-Src-mediated Twist Signaling, MicroRNA-10b Expression, and RhoA/RhoC Up-regulation, Leading to Rho-kinase-associated Cytoskeleton Activation and Breast Tumor Cell Invasion *. (2010) doi:10.1074/jbc.M110.162305.
18. Carvalho, M. P., Costa, E. C., Miguel, S. P. & Correia, I. J. Tumor spheroid assembly on hyaluronic acid-based structures: A review. Carbohydr Polym 150, 139–148 (2016).

19. Zhang, B. *et al.* 3D Bioprinting: A Novel Avenue for Manufacturing Tissues and Organs. *Engineering* vol. 5 777–794 Preprint at https://doi.org/10.1016/j.eng.2019.03.009 (2019).
20. Murphy, C. M. & O'Brien, F. J. Understanding the effect of mean pore size on cell activity in collagen-glycosaminoglycan scaffolds. *Cell Adhesion and Migration* vol. 4 377–381 Preprint at https://doi.org/10.4161/cam.4.3.11747 (2010).
21. Bružauskaitė, I., Bironaitė, D., Bagdonas, E. & Bernotienė, E. Scaffolds and cells for tissue regeneration: different scaffold pore sizes—different cell effects. Cytotechnology 68, 355 (2016).
22. Serafin, A., Culebras, M. & Collins, M. N. Synthesis and evaluation of alginate, gelatin, and hyaluronic acid hybrid hydrogels for tissue engineering applications. Int J Biol Macromol 233, (2023).
23. Pielesz, A. & Bąk, M. K. K. Raman spectroscopy and WAXS method as a tool for analysing ion-exchange properties of alginate hydrogels. Int J Biol Macromol 43, 438–443 (2008).
24. Serafin, A., Murphy, C., Rubio, M. C. & Collins, M. N. Printable alginate/gelatin hydrogel reinforced with carbon nanofibers as electrically conductive scaffolds for tissue engineering. Materials Science and Engineering C 122, (2021).
25. Saarai, A., Kasparkova, V., Sedlacek, T. & Saha, P. On the development and characterisation of crosslinked sodium alginate/gelatine hydrogels. J Mech Behav Biomed Mater 18, 152–166 (2013).
26. Vasvani, S., Kulkarni, P. & Rawtani, D. Hyaluronic acid: A review on its biology, aspects of drug delivery, route of administrations and a special emphasis on its approved marketed products and recent clinical studies. Int J Biol Macromol 151, 1012–1029 (2020).
27. Chen, H., Qin, J. & Hu, Y. Efficient Degradation of High-Molecular-Weight Hyaluronic Acid by a Combination of Ultrasound, Hydrogen Peroxide, and Copper Ion. Molecules 2019, *Vol. 24, Page 617* 24, 617 (2019).
28. Manju, S. & Sreenivasan, K. Conjugation of curcumin onto hyaluronic acid enhances its aqueous solubility and stability. J Colloid Interface Sci 359, 318–325 (2011).
29. Pérez, L. A., Hernández, R., Alonso, J. M., Pérez-González, R. & Sáez-Martínez, V. Hyaluronic Acid Hydrogels Crosslinked in Physiological Conditions: Synthesis and Biomedical Applications. Biomedicines 2021, *Vol. 9, Page 1113* 9, 1113 (2021).
30. Murphy, S. V., Skardal, A. & Atala, A. Evaluation of hydrogels for bio-printing applications. J Biomed Mater Res A 101 A, 272–284 (2013).
31. Mazzocchi, A., Devarasetty, M., Huntwork, R., Soker, S. & Skardal, A. Optimization of collagen type I-hyaluronan hybrid bioink for 3D bioprinted liver microenvironments. *Biofabrication* 11, (2019).
32. Pan, T., Song, W., Cao, X. & Wang, Y. 3D Bioplotting of Gelatin/Alginate Scaffolds for Tissue Engineering: Influence of Crosslinking Degree and Pore Architecture on Physicochemical Properties. J Mater Sci Technol 32, 889–900 (2016).
33. Li, Z. *et al.* Tuning Alginate-Gelatin Bioink Properties by Varying Solvent and Their Impact on Stem Cell Behavior. Sci Rep 8, (2018).

34. Rosell, R. *et al.* Non-small-cell lung cancer harbouring mutations in the EGFR kinase domain. *Clinical and Translational Oncology* vol. 12 75–80 Preprint at https://doi.org/10.1007/S12094-010-0473-0 (2010).
35. Zhang, F. *et al.* Fabrication of gelatin-hyaluronic acid hybrid scaffolds with tunable porous structures for soft tissue engineering. Int J Biol Macromol 48, 474–481 (2011).
36. Jaggupilli, A. & Elkord, E. Significance of CD44 and CD24 as Cancer Stem Cell Markers: An Enduring Ambiguity. *Clin Dev Immunol* 2012, 11 (2012).
37. Mesrati, M. H., Syafruddin, S. E., Mohtar, M. A. & Syahir, A. CD44: A Multifunctional Mediator of Cancer Progression. Biomolecules 2021, *Vol. 11, Page 1850* 11, 1850 (2021).
38. Wilson, G. S. *et al.* Efficacy of using cancer stem cell markers in isolating and characterizing liver cancer stem cells. Stem Cells Dev 22, 2655–2664 (2013).
39. Pandey, M. S., Harris, E. N., Weigel, J. A. & Weigel, P. H. The cytoplasmic domain of the hyaluronan receptor for endocytosis (HARE) contains multiple endocytic motifs targeting coated pit-mediated internalization. J Biol Chem 283, 21453–21461 (2008).
40. Trillsch, F. *et al.* E-Cadherin fragments as potential mediators for peritoneal metastasis in advanced epithelial ovarian cancer. British Journal of Cancer 2016 *114:2* 114, 213–220 (2016).
41. Juan, W., Shan, K., Na, W., Rong-Miao, Z. & Yan, L. The Associations of Genetic Variants in E-cadherin Gene With Clinical Outcome of Epithelial Ovarian Cancer. Int J Gynecol Cancer 26, 1601–1607 (2016).
42. Beavon, I. R. G. The E-cadherin-catenin complex in tumour metastasis: structure, function and regulation. Eur J Cancer 36, 1607–1620 (2000).
43. Ponta, H., Sherman, L. & Herrlich, P. A. CD44: from adhesion molecules to signalling regulators. Nat Rev Mol Cell Biol 4, 33–45 (2003).
44. Mao, M. *et al.* Effects of CD44 and E-cadherin overexpression on the proliferation, adhesion and invasion of ovarian cancer cells. Exp Ther Med 14, 5557 (2017).
45. Iseki, Y. *et al.* Significance of E-cadherin and CD44 expression in patients with unresectable metastatic colorectal cancer. Oncol Lett 14, 1025 (2017).
46. Xu, Y. & Yu, Q. E-cadherin negatively regulates CD44-hyaluronan interaction and CD44-mediated tumor invasion and branching morphogenesis. J Biol Chem 278, 8661–8668 (2003).

Figures

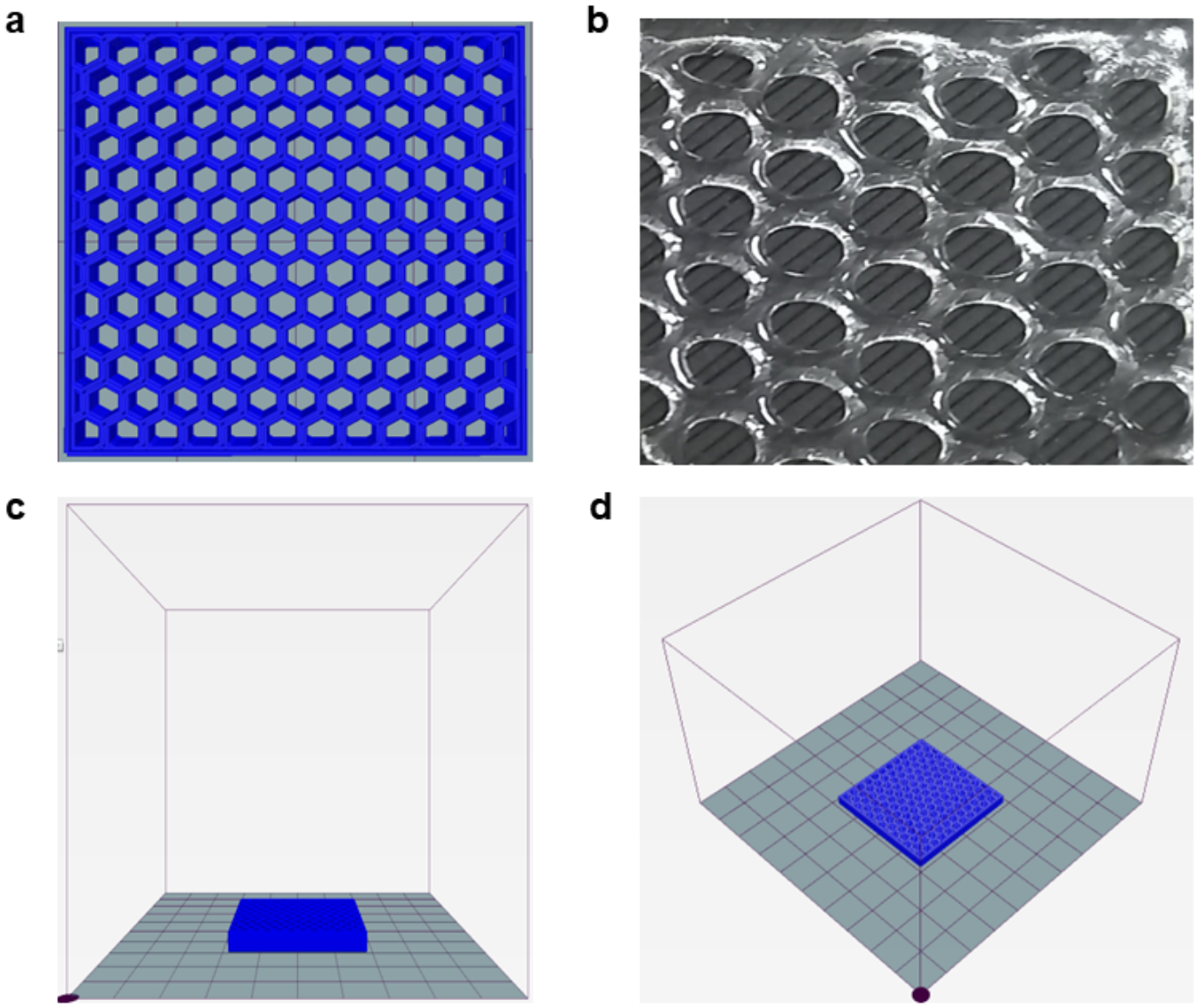

Figure 1

The three-dimensional scaffold created using alginate and gelatin in STL format image **(a)** view from the y-plane in STL format **(b)** the photograph image after printing, **(c)** view from the x-plane in STL format **(d)** view from the z-plane in STL format

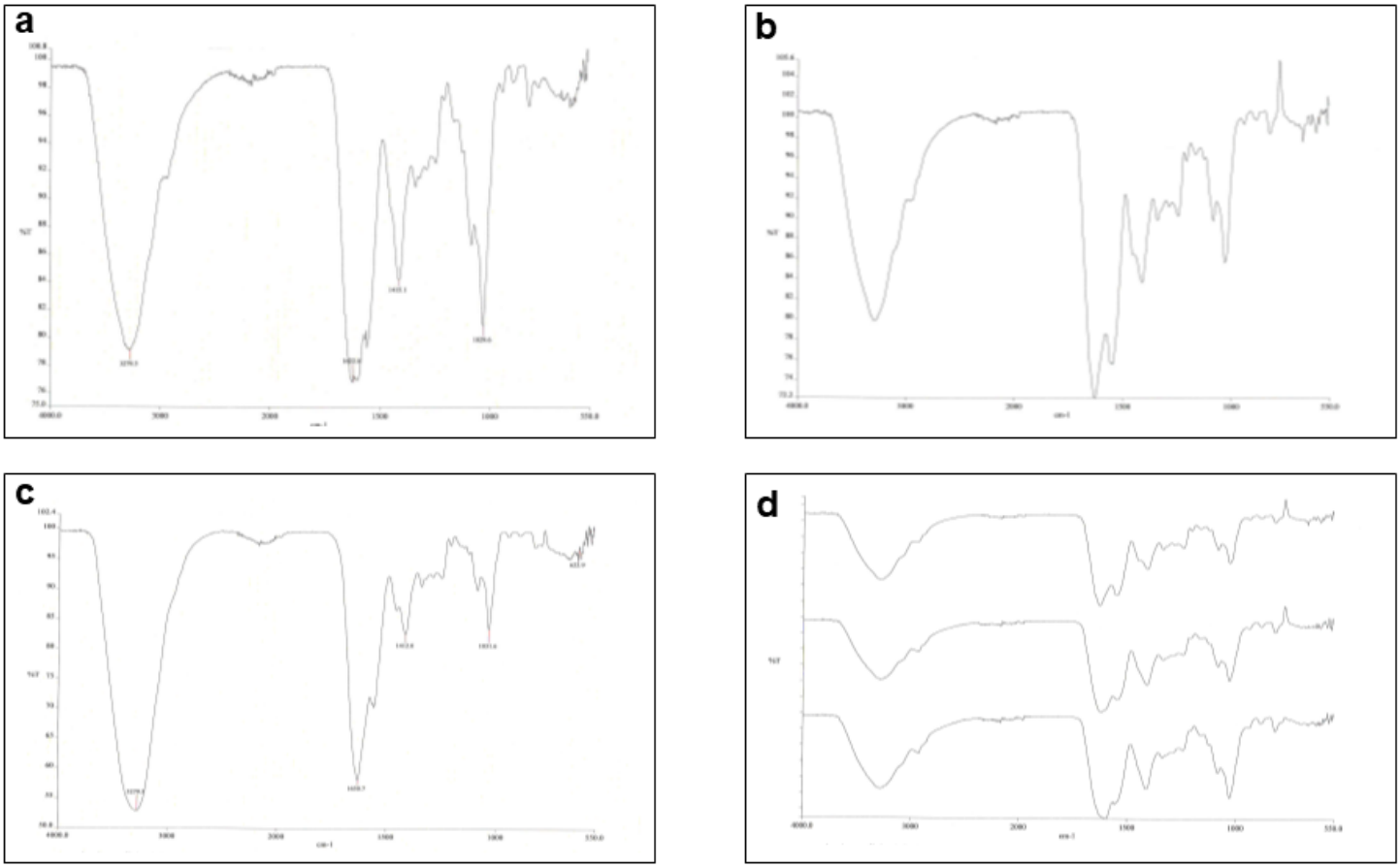

Figure 2

In scaffolds composed of alginate and gelatin, FTIR spectrometer measurement results were obtained for changes in HA concentration. **(a)** Alginate-gelatin scaffold with a 2% HA ratio. **(b)** Alginate-gelatin scaffold with a 1% HA ratio. **(c)**Alginate-gelatin scaffold with a 0,5% HA ratio. **(d)** Device library comparison results.

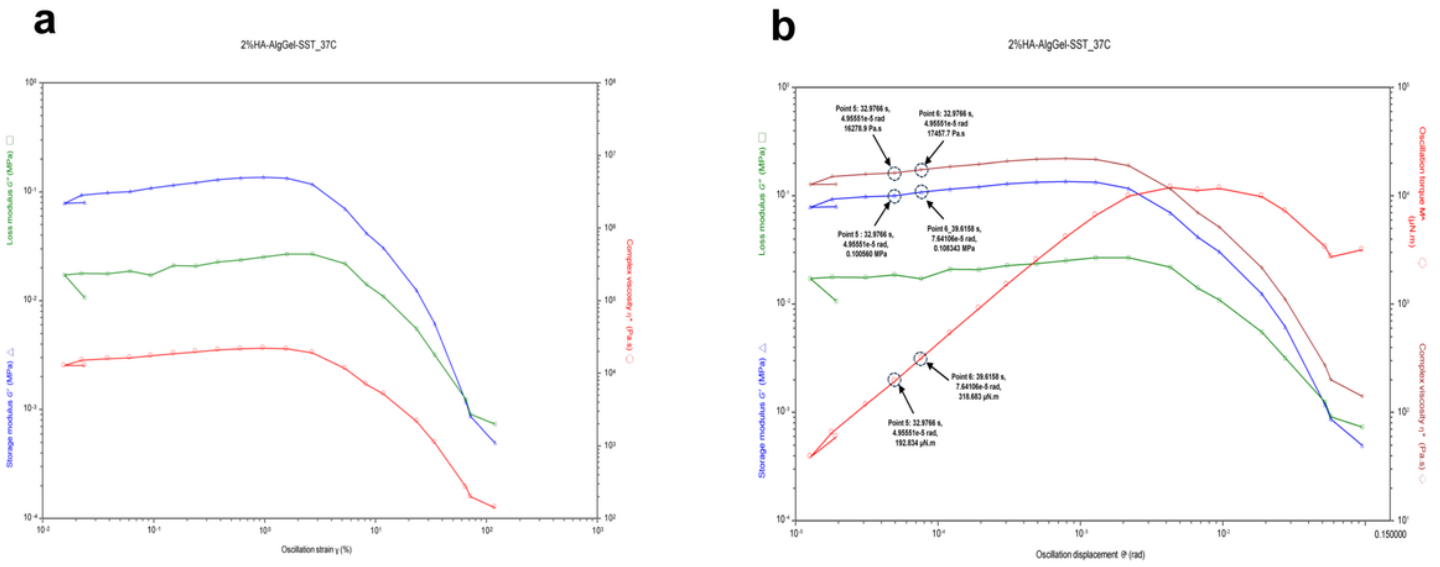

Figure 3

Rheological characterization of hydrogel mixtures containing 2% HA, 3% alginate, and 8% gelatin: **(a)** Storage modulus G' and loss modulus G" at different angular frequencies. The effect of increasing HA concentration on storage and loss moduli. **(b)** Viscosity of the hydrogel at different shear rates. The viscosity of the hydrogel mixture decreases with increasing shear rate.

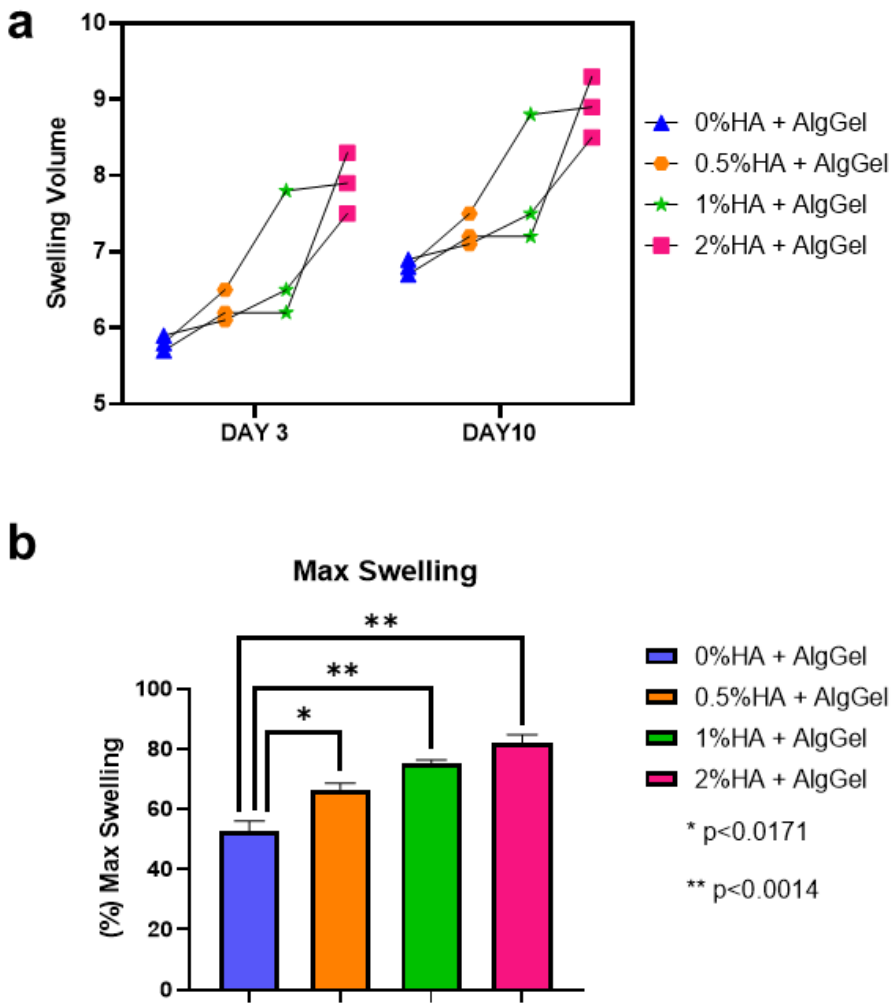

Figure 4

(a)in vitro biodegradation after various incubation times in PBS at 37 °C. **(b)** Swelling ratio of the hydrogels. Data are expressed as mean ± SD.While assessing the significance within the Live and Dead groups separately, a one-way ANOVA was used, *p<0.0171, ***p<0.0014.

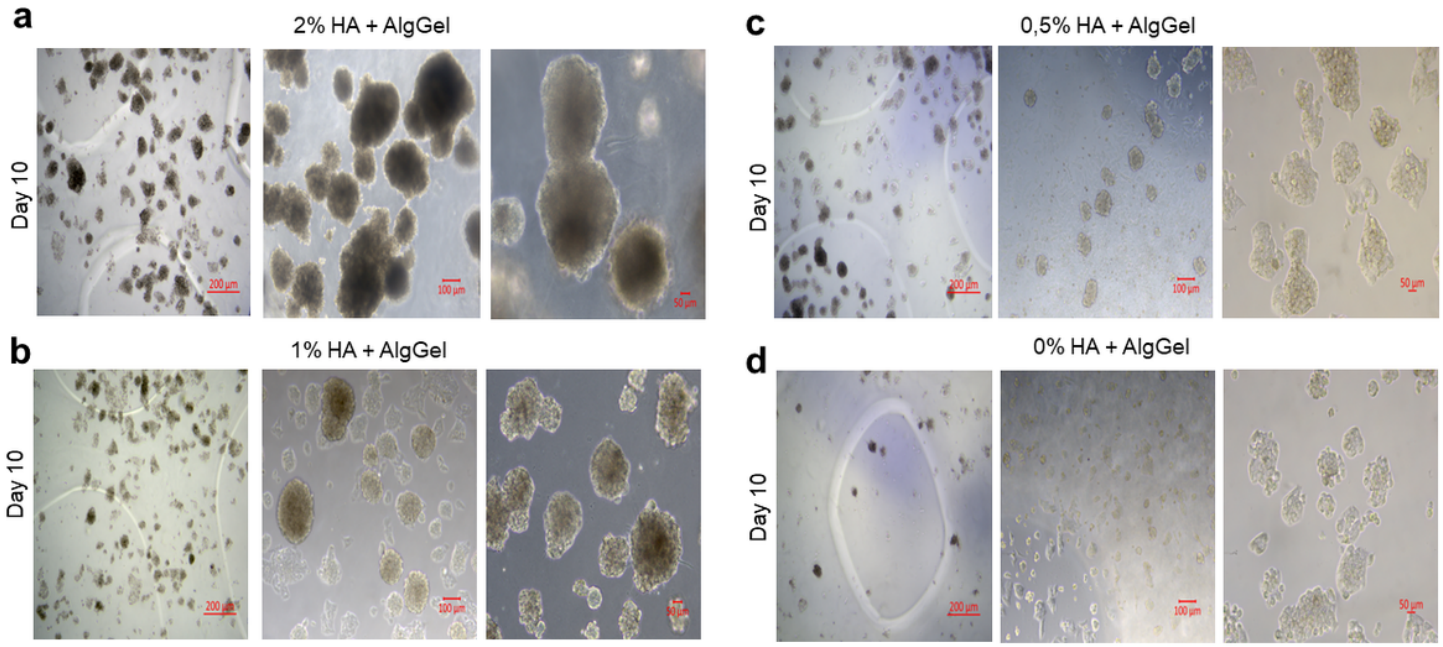

Figure 5

The formation of spheroids increases with the increase in the HA ratio. **(a)** HepG2 spheroids on scaffold containing 2% HA + AlgGel, **(b)** HepG2 spheroids on scaffold containing 1% HA + AlgGel, **(c)** HepG2 spheroids on scaffold containing 0.5% HA + AlgGel, **(d)** HepG2 cells on scaffold containing 0% HA + AlgGel. (The images were obtained with scale bars of 4X, 10X, and 20X, respectively.)

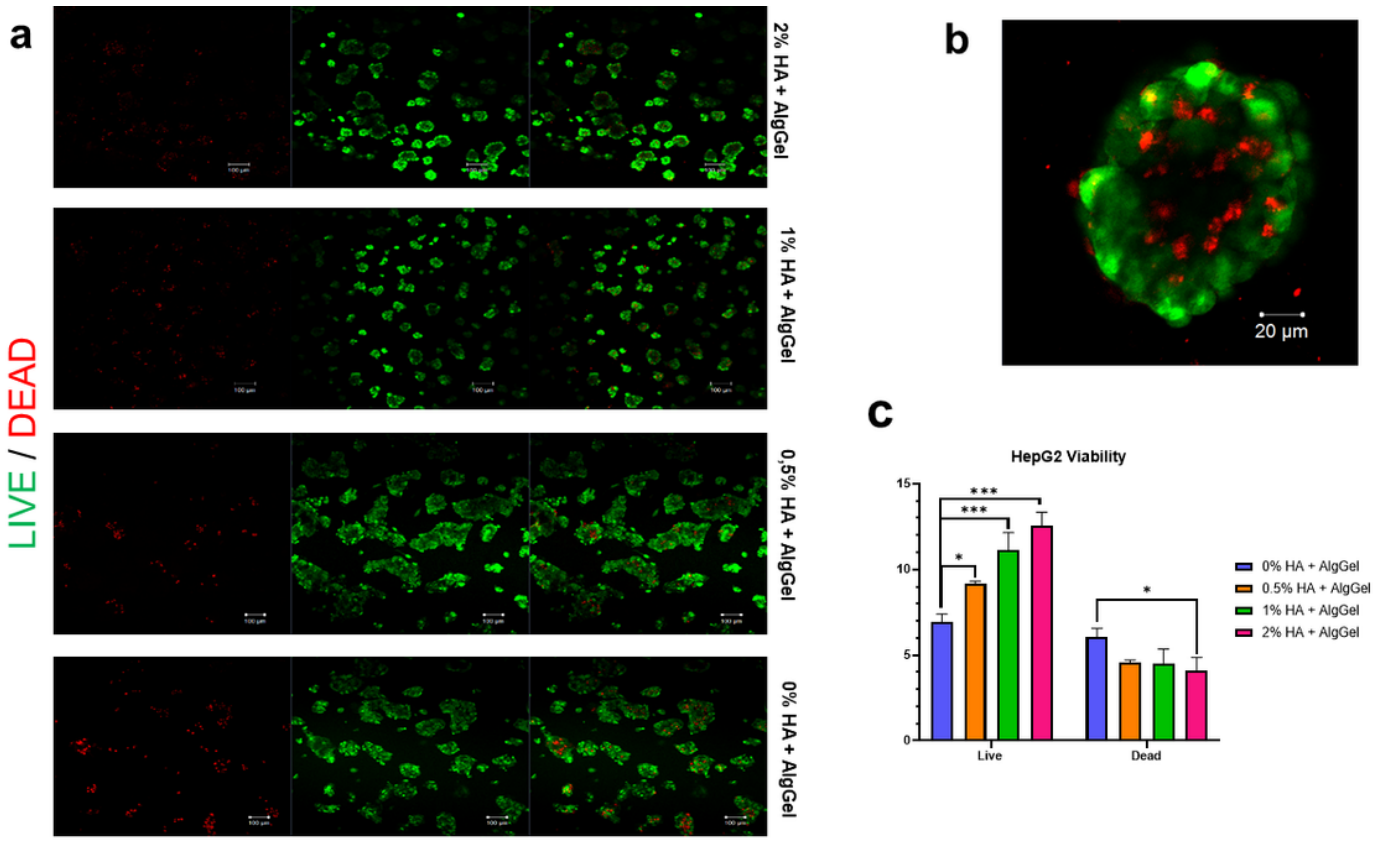

Figure 6

Cell viability in AlgGel scaffold at varying HA concentrations: **(a)** Live (green) and dead (red) cell images obtained through LIVE/DEAD imaging kit analysis, **(b)** Fluorescent images of live and dead cells within the scaffold forming spheroids, and **(c)** Quantification and graphical representation of live (Calcein AM) and dead (Bobo Iodide) cells using ImageJ. Data are expressed as mean ± SD. While assessing the significance within the Live and Dead groups separately, a two-way ANOVA was used, *p<0.0130, ***p<0.0001.

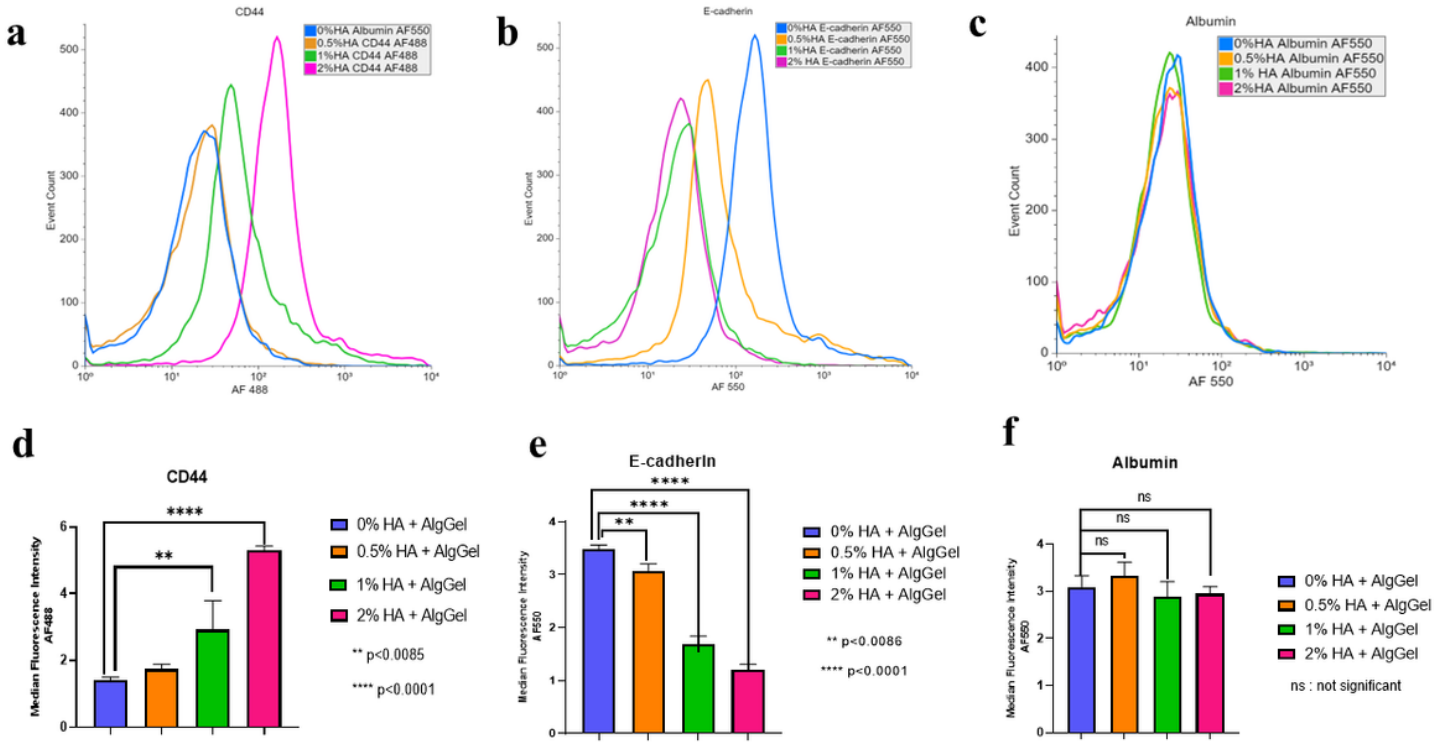

Figure 7

(a) Histogram graph of CD44 flow cytometer measurement, **(b)** histogram graph of E-cadherin flow cytometer measurement, **(c)** Histogram graph of Albumin flow cytometer measurement and Histogram graphs were prepared using the floreada.io program. **(d)** Statistical graph related to CD44 (**p<0.0085, ****p<0.0001), **(e)** statistical graph related to E-cadherin (**p<0.0086, ****p<0.0001) and **(f)** statistical graph related to Albumin, Statistical graphs were created using the Graphpad Prism program; one-way ANOVA was used to assess the significance between groups.

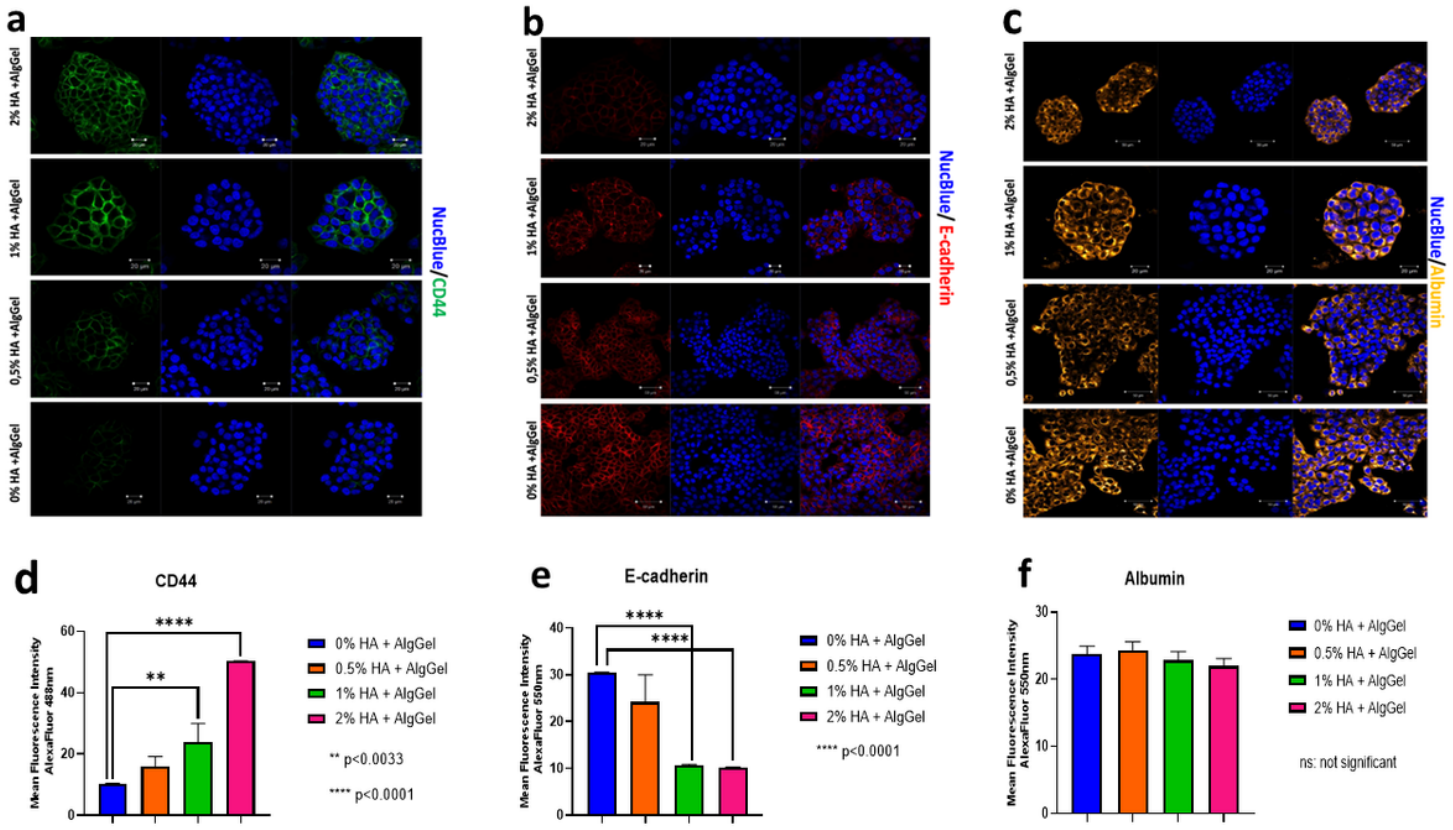

Figure 8

Confocal microscope images and mean fluorescence intensity graphs show the localization of CD44 **(a)**, E-cadherin **(b)**, and Albumin **(c)**in AlgGel scaffolds with varying concentrations of HA.Graphpad Prism program; one-way ANOVA was used to assess the significance between groups According to statistical values, the mean fluorescence intensity graphs for **(d)** CD44 (**p<0.0033, ****p<0.0001), **(e)** E-cadherin (****p<0.0001) and **(f)** Albumin are presented.

Supplementary Files

This is a list of supplementary files associated with this preprint. Click to download.

- Video1.DapiAlbuminCD44.mp4
- Video2.DapiAlbuminEcadherin.mp4